HIGH TEMPERATURE MECHANICAL PROPERTIES OF CMSX4+YTTRIUM SINGLE-CRYSTAL NICKEL-BASE SUPERALLOY

M. Marchionni*, D. Goldschmidt**, M. Maldini*
*CNR-ITM Cinisello B., Italy
**MTU Munchen GmbH, Germany

Abstract

CMSX4+Y, a highly strengthened rhenium-containing second generation single-crystal nickel-base superalloy, has been studied by creep as well as low cycle and thermomechanical fatigue in the temperature range of 500°C to 1100°C. The alloy exhibits very good high temperature mechanical properties better or comparable with other single crystal superalloys. The thermomechanical fatigue resistance is comparable with low cycle fatigue one and is cycle-shape dependent.

The observation of fracture surfaces shows that fracture induced by creep damage is internal and starts from pore-initiated cracks, while fatigue damage starts on the external surface and propagates inward in stage II mode.

Superalloys 1992
Edited by S.D. Antolovich, R.W. Stusrud, R.A. MacKay,
D.L. Anton, T. Khan, R.D. Kissinger, D.L. Klarstrom
The Minerals, Metals & Materials Society, 1992

Introduction

The continually increasing efficiency, durability and performance of aero-engines requires new materials exhibiting high mechanical resistance at elevated temperature. The development of single- crystal casting processes has led to the design of new superalloys from which components exhibiting excellent high temperature creep and fatigue resistance can be manufactured [1, 2].

In the first stages of aero-engine turbines the life-limiting factors for blades and vanes are oxidation, creep, thermal fatigue in the airfoil and low-cycle fatigue in the root section. In order to improve the high temperature properties, the oxidation resistance has been successfully increased by yttrium addition, even if the temperature of incipient melting and consequently the heat treatment window is thereby reduced [3, 4].

CMSX4, a highly strengthened rhenium-containing second-generation single-crystal nickel-base alloy, was modified by adding yttrium during the casting procedure [5]. The material properties were determined by analyzing the results of creep as well as low-cycle and thermomechanical fatigue at elevated temperatures and by investigating the damage micromechanisms involved.

Material and experimental techniques

The chemical composition of CMSX4+Y is given in Table 1. The alloy was heat-treated at 1290°C/1h + 1305°C/6h, then gas fast quenched which gives a fully γ' solutioned structure (no coarse γ') with some residual eutectic and a small amount of incipient melting (both <1%) (Figure 1). The incipient melting is due to a low melting point phase generated by the addition of yttrium to the base alloy. The alloy was aged at 1140°C/4h + 870°C/16h with the objective of creating cubic, well aligned, γ' particles of about 0.5 μm in size for optimum creep strength (Figure 2). Due to the very stable γ'-phase the first aging temperature had to be raised by 60°C in comparison with first generation alloys (e.g. SRR99). Deviations of <001> crystalline direction from the specimen axis were within 10°.

The creep specimens had a cylindrical geometry of 5.6mm diameter and 28mm gauge length. Three thermocouples were placed in the gauge length controlling and monitoring temperature gradients during creep.

Table 1 Chemical composition of CMSX4+Y alloy in weight %.

Ni	Co	W	Cr	Mo	Fe	Al	Ti	Ta	Hf	C	Re	Y(ppm)
60.5	9.5	6.3	6.4	0.6	0.1	5.5	0.9	6.3	0.08	0.007	2.9	50-150

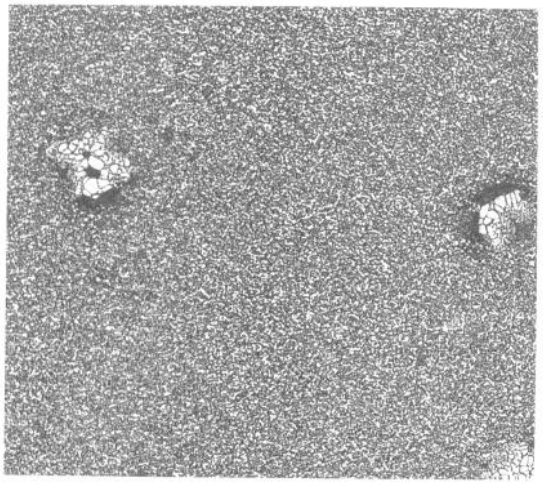

Figure 1 - Structure of CMSX4+Y alloy showing incipient melting zone.

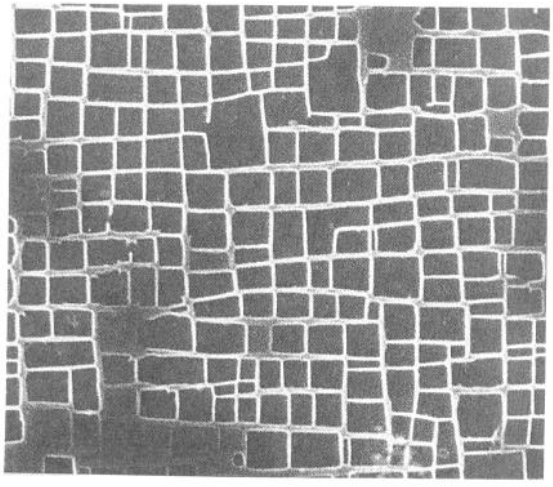

Figure 2 - Aspect of aligned γ' particles.

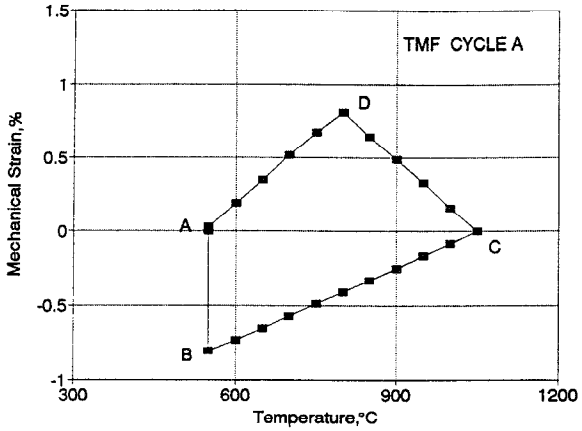

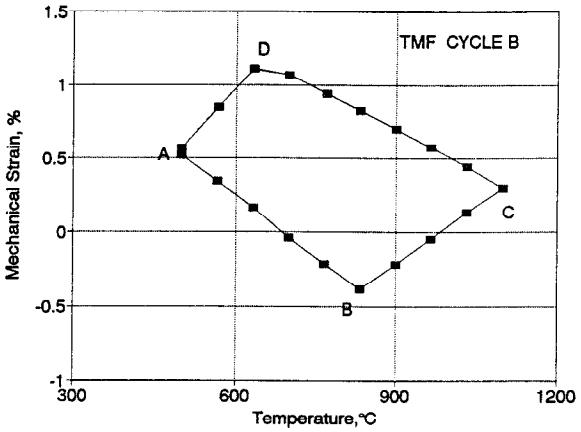

Figure 3 - Shape of thermomechanical cycle A. Figure 4 - Shape of thermomechanical cycle B.

Creep strain was continuously monitored using capacitive transducers connected to extensometers clamped to the shoulders of the specimen. Constant load and temperature creep tests were performed in the temperature range 850 - 1050°C and at nominal stresses selected to produce rupture times of 100 to 1500 h.

The low cycle fatigue (LCF) and thermomechanical fatigue (TMF) specimens were cylindrical with a diameter of 7mm and a gauge length of 12mm. The sample heating was made by induction coil and the temperature was controlled by thermocouples spot-welded outside the specimen gauge length. The LCF tests were carried out by specimens heated by induction coil at temperatures of 1000°C and 1100°C. The tests were performed under strain-controlled conditions at a strain rate of $3 \cdot 10^{-3} s^{-1}$ with a triangular wave form (R= -1). The TMF tests were performed by controlling temperature and strain variations selected to model the conditions of blades in service as close as possible. The Figures 3 and 4 shows the temperature and strain variations for cycles A (210 seconds) and B (180 seconds) respectively. During LCF and TMF tests the stress response and the hysteresis loop were recorded at intervals.

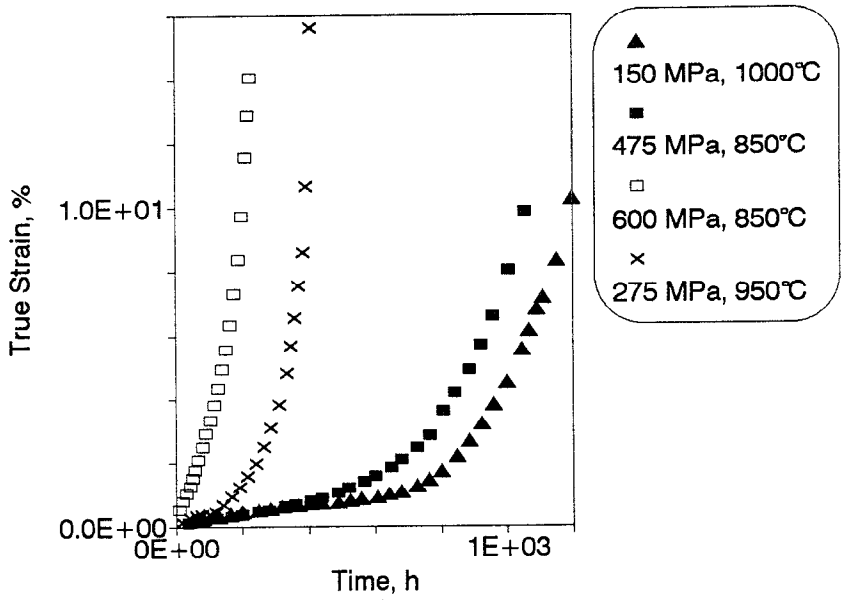

Figure 5 - Creep curves of CMSX4+Y alloy at different stresses and temperatures.

Experimental results and discussion

Creep results

The creep results are presented in Table 2.

A selection of typical creep curves is shown in Figure 5. CMSX4+Y, as many complex engineering alloys of interest for high temperature applications, exhibits a dominant accelerating creep stage, while primary and secondary stages are less important and sometimes negligible, both in amplitude and in duration. Such a behavior is better displayed in a plot of strain rate vs. strain (Figure 6), where a linear dependence of the strain rate on the strain is manifested up to 7-8%.

It should be emphasized that such a strain is reached after about 80-90% of the specimen creep life; after that final fracture mechanisms, e. g. crack propagation and/or localized reduction of area, can give an extra contribution of strain rate at the end of the creep curve. Equivalent behavior has been found in other single crystal superalloys [7, 8].

In Figure 7 the time to rupture vs. stress of the CMSX4+Y is compared with the SRR99 alloy, a typical first generation single crystal alloy; the better creep performance of the CMSX4+Y is evident.

Table 2 Creep results of CMSX4+Y alloy.

T, °C	σ, MPa	t_R, h	ε_R, %	Z_R, %
850	475	1165	18.5	21.7
	500	1090		
	525	661	19	20.8
	575	470		
	600	350		
	600	227	18.6	21.4
950	200	1304	24.1	26.4
	225	841	22.4	25.2
	250	498	22.8	25.1
	275	333	27.6	28.0
	300	191	20.8	26.1
980	210	540		
	225	385		
	250	241		
1000	150	1272	20.3	24.2
	200	287	18.4	23.3
	225	157	21.7	27.3
1050	140	520		
	140	414	22.8	32.7
	150	376		
	170	163		
	170	137	26.2	28.2
	180	110		

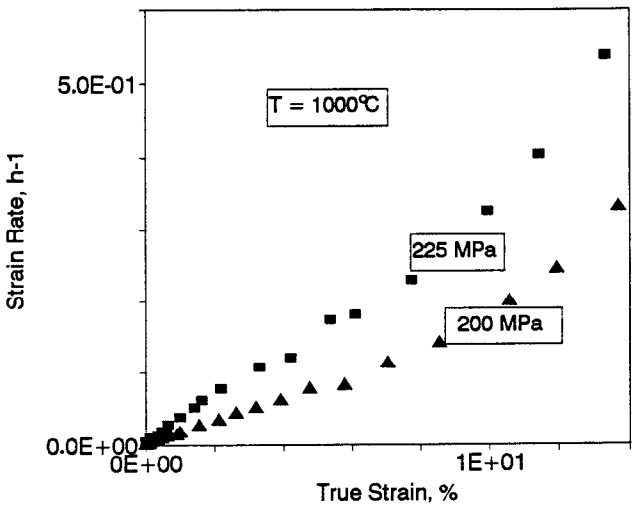

Figure 6 - Relation between strain rate and strain at different stresses.

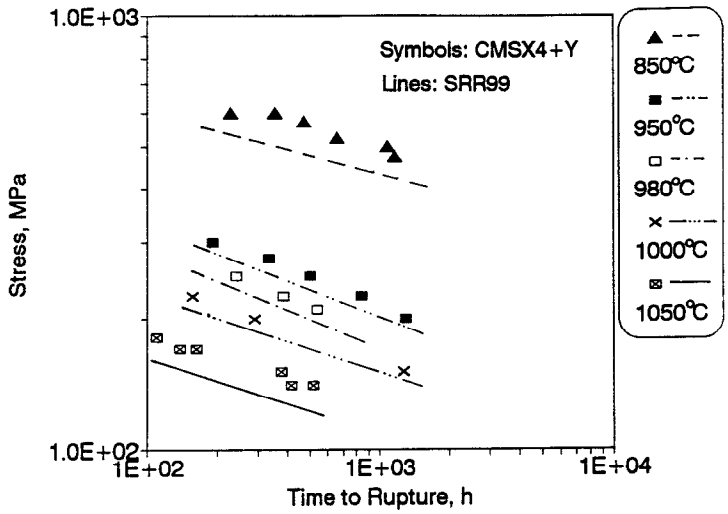

Figure 7 - Comparison of creep lives of CMSX4+Y and SRR99 [6] alloys at different temperatures.

LCF results

The LCF curves of CMSX4+Y alloy tested at 1000 °C plotted as total strain vs. number of cycles to failure are shown in Figure 8. The diagram presents the comparison of several single crystal alloys at 1000°C [9, 10, 11] in which CMSX4+Y alloy exhibits a fatigue life comparable with SRR99 single crystal, but better than other single crystal alloys. The temperature increasing to 1100°C reduces fatigue life sensibly only at low strain, but not at high strain.

The plots of elastic and plastic strain components vs. number of cycles to failure at 1000°C are reported in Figure 9. The plastic strain components are sensibly lower than the corresponding elastic ones owing to the low elasticity modulus in direction <001> that reduces sensibly the plastic zone in the hysteresis loop. Such a property increases sensibly the fatigue life in comparison with other policrystal nickel base superalloys [11]. The fatigue parameters are calculated according to the following Basquin [12] and Coffin Manson [13] equations:

$$\Delta\varepsilon_e = A \cdot N^{-\alpha} \quad (1)$$

$$\Delta\varepsilon_p = B \cdot N^{-\beta} \quad (2)$$

Table 3 Fatigue parameters of equations (1) and (2).

Temperature [°C]	A	α	B	β
1000	0.017	0.093	0.023	0.40
1100	0.028	0.19	0.12	0.52

where $\Delta\varepsilon_e$ and $\Delta\varepsilon_p$ are the elastic and plastic strain components, N the number of cycles to failure, A, α, B and β constants of the material. The values obtained are reported in Table 3.

The influence of test temperature is shown in Fig. 10. The temperature increasing reduces fatigue life sensibly at low strains, while it is less sensible at high strain.

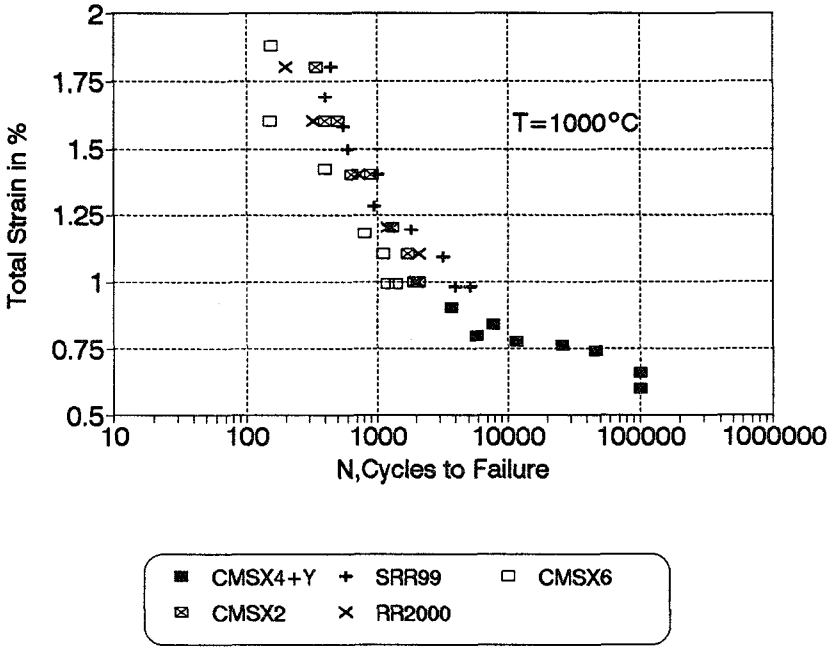

Figure 8 - Comparison of LCF lives for different single crystal alloys.

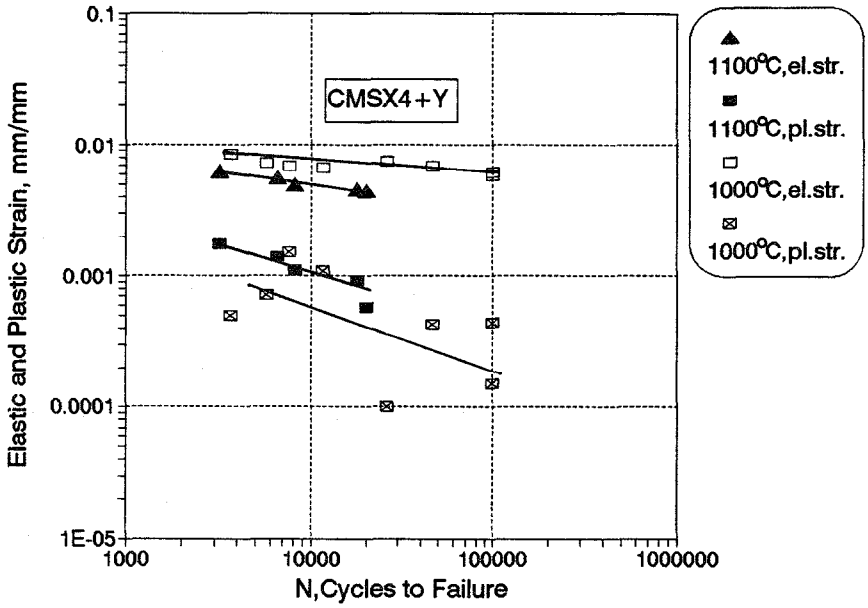

Figure 9 - Elastic and plastic strain vs. cycles to failure.

TMF results

The TMF results are compared with LCF curves in Figure 10. The cycle A of Figure 3 was selected in order to obtain a symmetrical strain variation similar to that of LCF tests, while cycle B of Figure 4 was established as close as possible to that observed in service. Since simulation of the actual strain-temperature cycle of operational component is too time-consuming, we have chosen a diamond-shape cycle B with the maximum (1100°C) and minimum (500°C) temperatures typical of component application, but with the applied cyclic strains considerably higher than those indicated by the component stress analysis results.

The number of cycles to failure observed in TMF tests with cycle A is comparable to that observed in low-cycle fatigue tests at highest temperature and indicates that fatigue damage is equivalent in both cases. When the cycle B is applied, the fatigue life is sensibly increased probably due to the maximum tensile strain that occurs at a temperature 200°C lower than that corresponding to the maximum tensile strain of cycle A. In this case fatigue life prediction using only LCF results could be too conservative. An example of hysteresis loop with cycle B in shown in Figure 11.

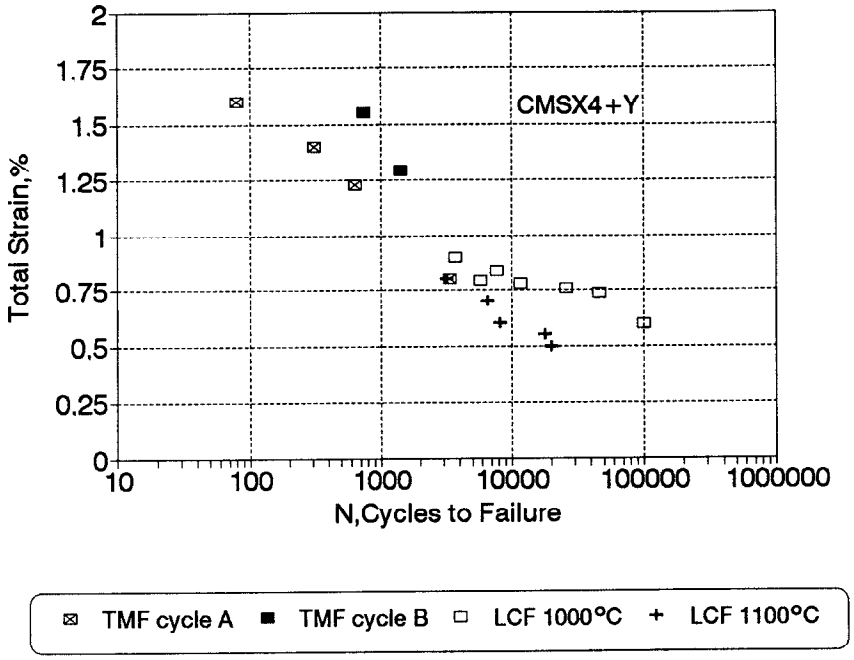

Figure 10 - Comparison of LCF and TMF endurances.

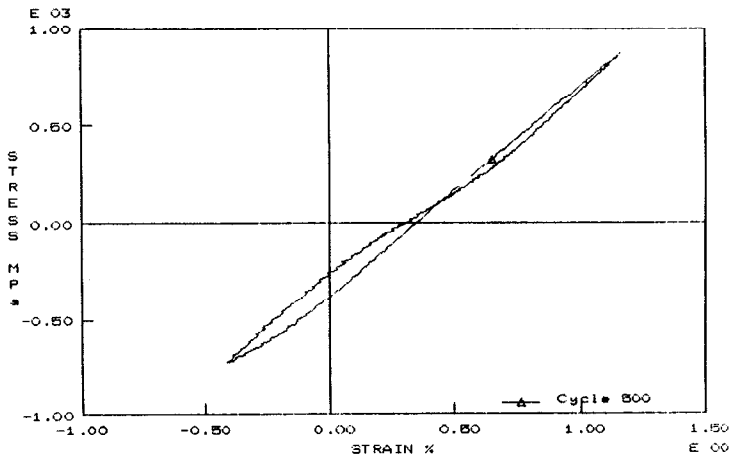

Figure 11 - Example of TMF hysteresis loop: cycle B, $\Delta\varepsilon_m$=1.16%, N=740.

Metallography

The creep fracture surfaces and a longitudinal section of crept specimens have been examied by SEM.

As found in other single crystal nickel base superalloys [14, 15] creep cracks initiate almost always at casting pores located between dendrite arms, and slowly propagate anisotropically along planes, perpendicularly to the applied stress (Figure 12, 10U=100μm). Figure 13 shows the morphology of creep fracture surfaces. At the lowest temperatures they consist mainly in square-like facets oriented on <001> planes while at increasing temperature the facets become progressively rounded. Metallographic measurements of crystalline orientation showed that the four edges of the facets were <110> and <1$\bar{1}$0> directions. This creep crack behavior is consistent with the fractography of CMSX2, SRR99 and RR2000 [15].

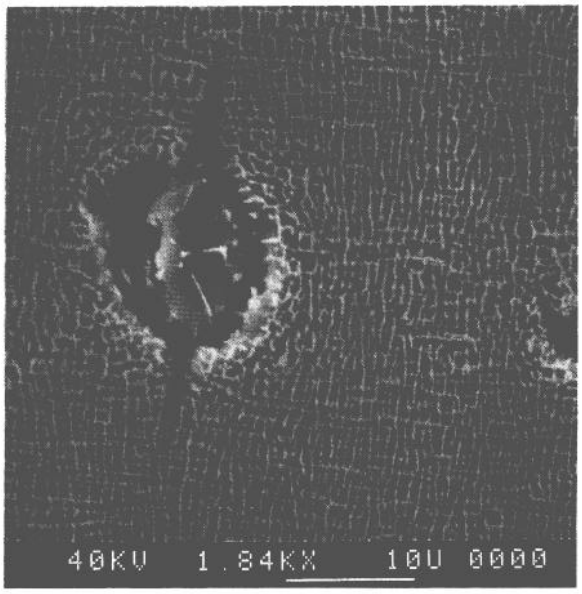

Figure 12 - Example of pore crack initiation T=950°C, 225MPa, 841h.

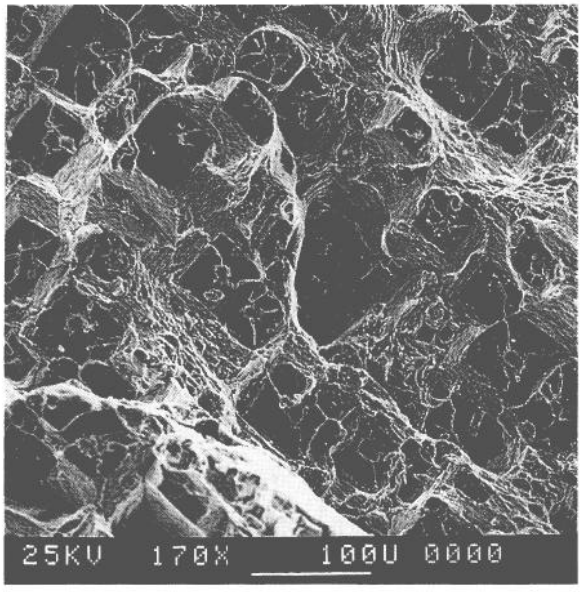

Figure 13 - Creep fracture surface aspect: sqare-like facets are visible, T=850°C, 600MPa, 227h.

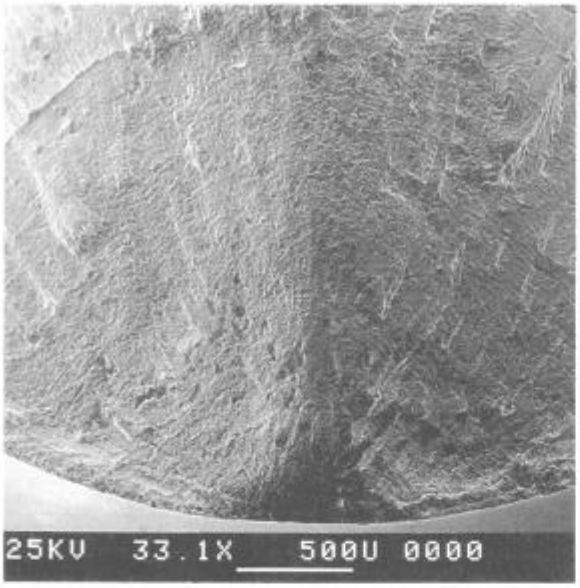

Figure 14 - Example of LCF fracture surface: T=1100°C, $\Delta\varepsilon_t$ =0.8%, N=3,200.

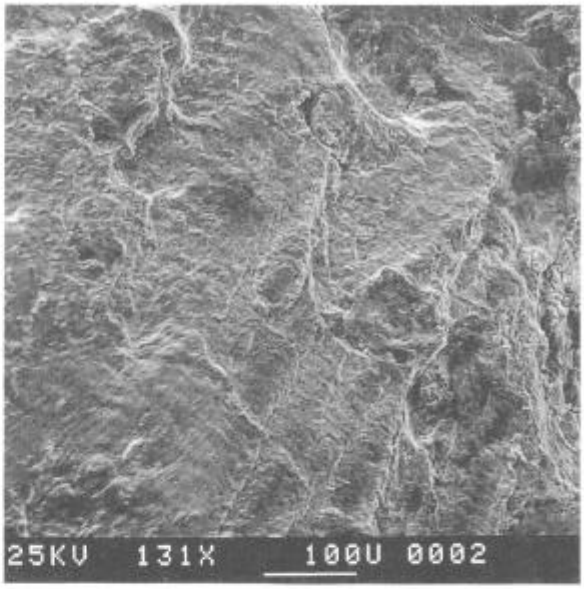

Figure 15 - Fatigue striations covered by a thick oxide layer in the same specimen of the previous figure.

Also the LCF and TMF fractures have been observed by SEM. Generally the crack (or cracks) nucleates on the external surface of the specimen and propagates inward in stage II mode. The morphology of fracture surfaces is similar even if the time per cycle is sensibly different in TMF and LCF tests. An example of LCF crack initiation and propagation is shown in Figure 14. Inward the fracture surfaces fatigue striations have been found. They are less visible at 1100°C due to the presence of a thick oxide layer (Figure 15). Striations have been found also in specimens fractured by TMF test (Figure 16), and the fracture exhibits an oxidation layer less pronounced. In our experiments crack initiation in LCF and TMF is always external, except for a TMF specimen tested at very low strain for 3348 cycles and then subjected to higher strain for 80 cycles until fracture occurred: in the fracture surface secondary cracks, initiated from internal pores, can be observed (Figure 17).

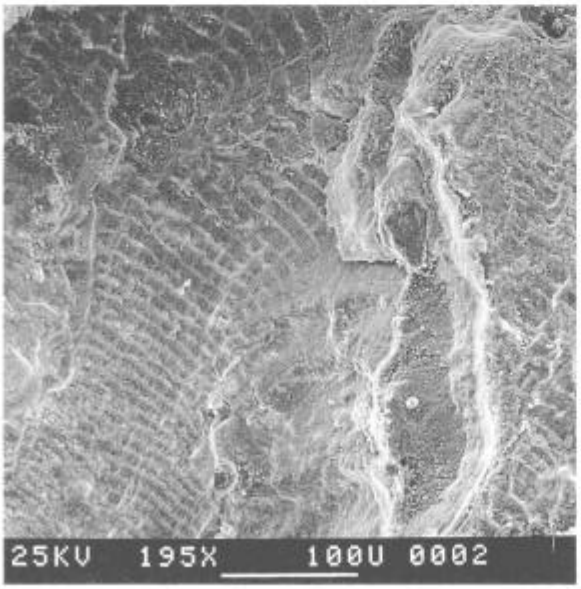

Figure 16 - Example of fatigue striations after TMF: cycle B, $\Delta\varepsilon_m$=0.97%, N=1420.

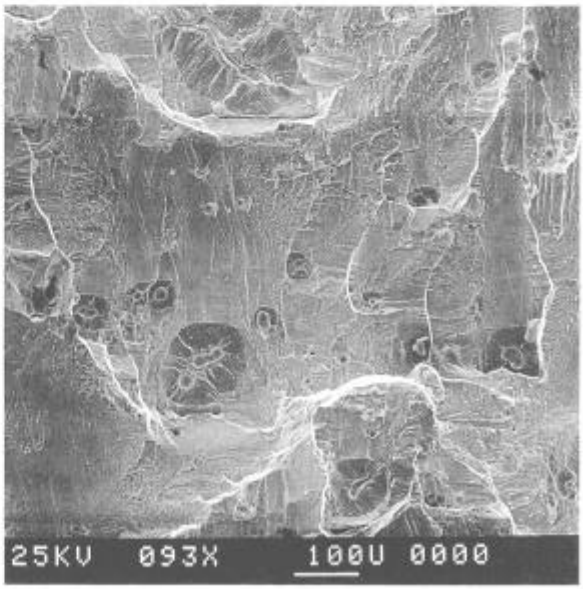

Figure 17 - Example of cracks pore-derived after TMF: cycle A, $\Delta\varepsilon_m$=0.8%, N=3348.

Concluding remarks

Creep, LCF and TMF tests on CMSX4+Y single crystal superalloy at different temperatures show:
- The alloy exhibits comparable or better high temperature mechanical properties than other single crystal nickel base superalloys;
- TMF tests performed with cycle A and LCF tests performed at 1100°C show a comparable endurance, while TMF tests performed with cycle B present better fatigue life;
- creep fractures initiate from internal pores only at the last few per cent of creep life and cracks consist mainly in square-like facets oriented on <001> planes;
- LCF and TMF fractures start on the outside and propagate inward in stage II mode with the presence of fatigue striations;
- TMF fractures obtained at low strains exhibit the presence of internal secondary cracks initiated from pores similar to those observed in crept specimens.

Acknowledgments

Authors acknowledge gratefully Mr. E. Picco, Mr. D. Ranucci, Mr. E. Signorelli, Mr. D. Valenti of ITM and Mr F. Zarda of MTU for the experimental activity.

The work has been performed as a part of the European Concerted Action Cost 501 second round programme.

References

1. K. Harris, G. L. Erickson, and R. E. Schwer, Development of the CMSX* series of single crystal alloys for advanced technology turbine components, TMS-AIME Fall Meeting, St. Louis, Missouri, (27 October 1982).

2. K. Harries, G. L. Erickson, and R. E. Schwer, CMSX Single Crystal, CMDS & Integral Wheel Alloys Properties & Performance, in Proc. of "High Temperature Materials for Power Engineering 1986", Cost 50/501 conference, (ed Betz et al., Liège, October 1986).

3. P. Hupfer, Spurenelemente in Superlegierungen, Fachberichte Hüttenpraxis Metallweiterverarbetung, No. 9, (1989), 24, 773.

4. F. D. Hondros, The Magic of Active Elements in the Oxidation Behaviour of High Temperature Metals and Alloys, (ed Lang, Petten, 1989), XI.

5. F. Meyer-Olbersleben: Thermal Fatigue of an Yttrium-Modified Single Crystal Superalloys, to be presented at LCF3 International Conference, Berlin, (7-11 September 1992).

6. L. W. Candler, and M. R. Winstone, Proc. of International Conference of "High Temperature Materials for Power Engineering", (Liège 1990), 1971.

7. M. Maldini, and V. Lupinc, Scripta Metall., 22 (1988), 1737.

8. V. Lupinc, M. Maldini, and V. Catena, Evolution of Advanced Materials, AIM/ASM, Milano, (1989), 161.

9. V. Lupinc et al., Nuove Superleghe a Struttura Direzionale per Palette di Turbine a Gas Avanzate, La metallurgia Italiana Vol. 81, N. 10, (1989), 825.

10. M. Marchionni et al., Fatica Oligociclica ad Elevata Temperatura di una Superlega di Nichel Monocristallina Tipo CMSX2, Proc. of XVIII Convegno Nazionale AIAS, (Amalfi, 1990), 571.

11. M. Marchionni et al. High Temperature Low Cycle Fatigue of Single Crystal Nickel Base Superalloys, Proc. of "Fatigue '90" International Conference, (Honolulu, Hawai, 1990), 1735

12. Basquin O. H., The Exponential Law of Endurance Tests, Proc. ASTM 10, 1910, 625.

13. Coffin L. F. Jr., Fatigue at High Temperature, ASTM STP 520, 1972, 12.

14. A. A. Hopgood, J. W. Martin: Materials Science and Engineering, 82 (1989) 27-36.

15. S. H. Ai, V. Lupinc, M. Maldini, Scripta Metall., 26 (1992) 579.